Thermal Spin Torque in Double-Barrier Tunnel Junctions with Magnetic Insulators

Christian Ortiz Pauyac,[1] Collins Ashu Akosa,[1,2,3,*] Gen Tatara,[1,2] Mairbek Chshiev,[4,5] and Alan Kalitsov[6]

[1] *RIKEN Center for Emergent Matter Science (CEMS), 2-1 Hirosawa, Wako, Saitama 351-0198, Japan*
[2] *RIKEN Cluster for Pioneering Research (CPR), 2-1 Hirosawa, Wako, Saitama 351-0198, Japan*
[3] *Department of Theoretical and Applied Physics, African University of Science and Technology (AUST), Km 10 Airport Road, Galadimawa, Abuja F.C.T., Nigeria*
[4] *Univ. Grenoble Alpes, CEA, CNRS, Spintec, 38000 Grenoble, France*
[5] *Institut Universitaire de France (IUF), 75231 Paris, France*
[6] *Western Digital, San Jose, California 95131, USA*

(Received 19 November 2020; revised 26 April 2021; accepted 3 May 2021; published 1 June 2021)

The thermal spin torque induced by the spin-dependent Seebeck effect in double-barrier tunnel junctions is derived considering free-electron and tight-binding calculations. We show that in systems comprising ferromagnetic electrodes and nonmagnetic barriers, the in-plane component of the thermal spin torque is the dominant term, whereas in junctions comprising nonmagnetic electrodes and ferromagnetic barriers, both components, the in-plane and the out-of-plane, are comparable in magnitude. Moreover, larger torque amplitudes up to 3 orders of magnitude are obtained in the second system as a result of the spin-filtering effect; consequently, double-barrier tunnel junctions in the presence of magnetic insulators offer an enhanced thermal spin-torque mechanism for reliable applications. We propose taking advantage of quantum resonant tunneling through resonance states below the Fermi level in these structures that can pave a route toward achieving larger spin-torque efficiencies, even when considering smaller values of the exchange splitting. Furthermore, we identify the parameters needed to tune efficiently these resonant states.

DOI: 10.1103/PhysRevApplied.15.064003

I. INTRODUCTION

Over recent years, there has been enormous progress in spintronics toward realizing the next generation of high-density nonvolatile memories, logic chips, and magnetic sensors with low critical currents and high thermal stability; however, the nanosize nature of such devices has rendered them less stable as a result of extensive heating. To overcome this, the exploitation of undesired thermal losses to reduce energy consumption has been proposed, which constitutes, in recent years, the fundamental motivation for the development of clean and sustainable thermoelectric functioning devices. This has become the subject of a field called spin caloritronics [1] that deals, in contrast to conventional spintronics, with the generation of charge and spin currents induced by temperature gradients (and vice versa). Most of the recently uncovered phenomena in this field are centered around the spin Seebeck (SSE) [2] and the spin-dependent Seebeck (SDSE) [3] effects. The former, studied in permalloys [4], magnetic insulators [5], ferromagnetic semiconductors [6], and Heusler alloys [7], originates from collective effects that involve electronic and magnonic spin currents. It has given rise to important phenomena such as thermally induced spin pumping [8] and thermally induced spin torque [9]. The latter, studied in magnetic heterostructures, is purely electronic in nature, i.e., a heat current couples to a charge current with two parallel spin transport channels and therefore it involves the thermoelectric generalization of collinear magnetoelectronics. It has led to important effects such as Seebeck spin-tunneling [10], magneto-Peltier cooling [11], the magneto Seebeck effect [12,13], and thermal spin-transfer torque (TSTT). Note that both SSE and SDSE give rise to thermal torques. In this work, we focus on the one arising from SDSE, which, in contrast to the conventional current-induced case [14], considers a thermally excited spin current to generate a torque. It has been predicted in metallic spin valves [15], followed by experimental observations on Co/Cu/Co samples [16,17]. Later, Yuan *et al.* have shown that considering temperature gradients of 1 K on Ni and Co domain walls is sufficient to generate TSTT amplitudes comparable with those of the current-induced case [18], indicating the considerable potential of thermal spin-transfer torques for spin-based

*collins.akosa@riken.jp

memories and energy harvesting. In magnetic tunnel junctions (MTJs), TSTT has been studied by Jia *et al.* [19], followed by experimental measurements in Co-Fe-B/MgO layers [20,21]. Since then, most of the effort has been oriented toward the development of MgO-based MTJs for thermally induced magnetization dynamics [22,23], which can have a strong impact in magnetic recording applications [24]. It has been found that MTJs, in the presence of thermal gradients, exhibit a strong energy dependence of the electron transmission due to the existence of interface resonant states [25,26]. This becomes visible considering Sommerfeld expansion, where the expectation values of observable A, $\langle\rangle$, in the presence of an external bias voltage and a temperature gradient read $\langle A\rangle_{\Delta V} \propto \hat{a}$ and $\langle A\rangle_{\Delta T} \propto \partial_E \hat{a}$, respectively. The energy derivative in the thermal case, ∂_E, applied on the operator $\hat{a}$, gives a strong indication that band-structure engineering and, in particular, coherent resonant transport can in principle lead to enhanced thermoelectric effects. One direction has been successfully applied in Ref. [27], where the authors have exploited resonant states at the interfaces of (Fe-Co)/MgO MTJs in order to enhance the thermoelectric power and its related thermal spin conductivity. A second direction is exploited in this work, where we consider double-barrier structures that give rise to resonant tunneling effects due to the formation of quantum wells between the barriers. Two types of systems are studied, (i) double magnetic tunnel junctions (DMTJs) and (ii) double-spin-filter tunnel junctions (DSFTJs). The former comprises ferromagnetic electrodes and nonmagnetic barriers sandwiched with a metallic spacer. On the other hand, the latter considers nonmagnetic electrodes and magnetic barriers. The DMTJ has been studied in the presence of external bias voltages [28,29] and soon extended to thermal gradients. Considering nonmagnetic spacers, Ref. [30,31] has reported TSTT amplitudes twice as large as that of traditional single-barrier MTJs, whereas considering ferromagnetic spacers in Ref. [32], lower temperature gradients have been needed to switch the magnetic configuration. In both studies, however, no analytical expressions have been provided. In this work, we address a similar system and support our findings with analytical calculations. Regarding the DSFTJ, this is an alternative configuration, with the use of magnetic insulators as barriers. In the presence of thick barrier layers, the electronic transport across the sample is suppressed and the system reduces to a magnonic spin valve, where the spin Seebeck effect induced by the temperature difference creates a magnon current that depends on the relative orientation of the magnetic layers magnetizations [33,34]. Magnon-current generation in magnetic insulators has attracted increasing interest for providing long-distance propagation of spin information without Joule heating [35]. It has also led to magnonic spin-transfer torques in architectures such as magnonic spin valves [36], domain walls [37,38], and MTJs [39–42]. However, when considering thin barrier layers, not only does the magnonic current decrease but also the electronic tunneling current emerges. This current, in thin magnetic insulators such as Eu chalcogenides [43–45] or spinel-based materials [46–51], is driven by the spin-filtering effect, which selectively filters majority carriers due to the spin-dependent evanescence of the wave function in the barrier [52] and has been shown to contribute to larger torque amplitudes compared to conventional MTJs [53]. In the presence of two magnetic insulators with misaligned magnetizations, the electronic spin-polarized current generated in one layer exerts a torque in the second one. This has been studied in the presence of external bias voltages, either considering fully insulating junctions [54] or metallic spacers [55], but has mostly been overlooked in the presence of thermal gradients. In this work, we address the thermal case, neglecting the contribution of the magnon current, which has been shown to be additive [56], and therefore we focus instead on the electronic transport differences between DMTJs and DSFTJs. Our results show that the latter exhibit larger torque amplitudes that can be efficiently exploited considering coherent resonant tunneling.

II. MODEL

We consider double-barrier tunnel junctions of the form $L/B_1/S/B_2/R$, where L and R denote semi-infinite left and right leads, B_1 and B_2 represent the barrier region, and S is the metallic spacer. Two cases are considered: (i) ferromagnetic (FM) leads attached to nonmagnetic barriers (I) and (ii) nonmagnetic (NM) leads attached to ferromagnetic barriers (FI), shown in Figs. 1(a) and 1(b), respectively. In the absence of S, the former reduces to a conventional MTJ (FM/I/FM), whereas the latter reduces to a single layer spin-filter tunnel junction (NM/FI/NM). The system is subjected to a thermal difference, i.e., $\Delta T = T_R - T_L$, where $T_{R(L)}$ denotes the temperature on the right (left) lead. The magnetization vector on R (B_2) is fixed along the z axis, whereas the one on L (B_1) is oriented on the x-z plane with angle θ [see Figs. 1(a) and 1(b)], where we choose $\theta = \pi/2$. We calculate the local charge and spin-current densities, which are denoted as $\mathbf{j}$ and $\mathbf{J}$, respectively. For transport given along y, the spin-current density has three nonzero components, J_y^x, J_y^y, and J_y^z, where the superscripts and subscripts refer to the spin and real space, respectively. Conventionally, these components are related to the appropriate spin-torque components [57–59]. In systems made of ferromagnetic leads attached to nonmagnetic barriers, we calculate the spin-torque components on the right semi-infinite ferromagnetic lead; these components, in-plane ($T_\parallel$) and out-of-plane ($T_\perp$), estimated per unit area, are equal to the spin-current density components at the B_2/R interface,

$$T_{\parallel(\perp)} = \langle J_{y_r}^{x(y)} \rangle. \tag{1}$$

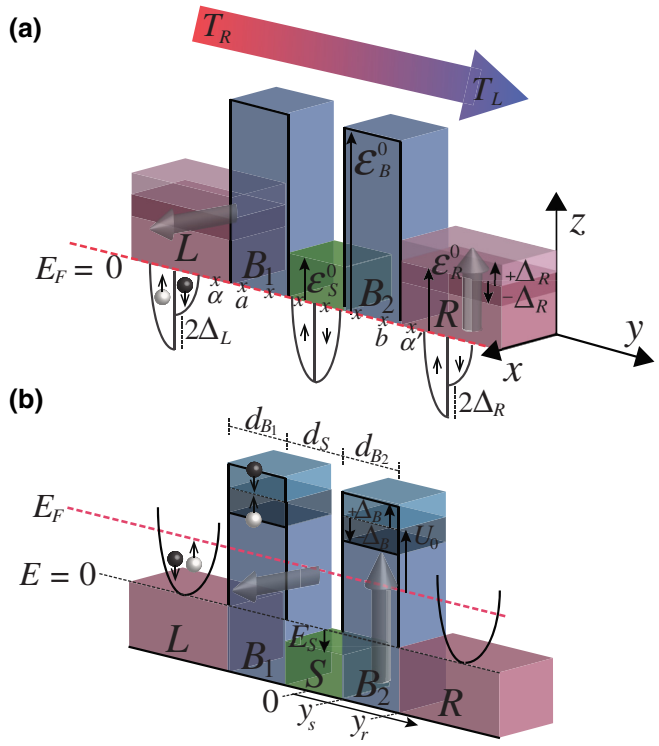

FIG. 1. Schematic illustration of our systems. (a) The tight-binding potential profile of a double-barrier MTJ (FM/I/NM/I/FM). ϵ_Ω^0 is the averaged on-site energy in Ω. $\Delta_{L,R}$ indicates the exchange splitting in the leads, E_F is defined at zero. (b) The free-electron potential profile of a double-barrier spin-filter junction (NM/FI/NM/FI/NM). E_F is the Fermi energy, $U_0 + E_F$ is the barrier height, Δ_B is the exchange splitting in the barrier, E_S is the spacer height relative to the leads, and $d_{B_i(S)}$ is the barrier (spacer) width. Both systems are subjected to a temperature gradient $T_R - T_L$.

In contrast, in systems made of nonmagnetic leads attached to ferromagnetic barriers, these components are calculated on B_2 and therefore we have

$$T_{\parallel(\perp)} = \langle J_{y_s}^{x(y)} \rangle - \langle J_{y_r}^{x(y)} \rangle, \tag{2}$$

where $y_{s(r)}$ refers to the position of the $S|B_2(B_2|R)$ interface along the transport axis and $y = 0$ is defined at the center of the spacer region [see Fig. 1(b)]. In this work, two models are employed to study the thermal spin-torque components: (i) the free-electron model and (ii) the tight-binding model.

A. Free-electron model

The wave functions in the metallic regions are plane waves of the form

$$\Psi_\Omega^\sigma(y) = a_\Omega^\sigma \exp(ik_\Omega^\sigma y) + b_\Omega^\sigma \exp(-ik_\Omega^\sigma y). \tag{3}$$

Ω represents the L, R, or S region and $\sigma = \uparrow (+1)$ or $\downarrow (-1)$ is the spin-up or spin-down projection, respectively. The wave vectors are given by $k_\Omega^\sigma = \sqrt{(2m/\hbar^2)(E_\perp + \sigma\Delta_\Omega - \mu_\Omega)}$. Δ is the exchange splitting, μ is the chemical potential, and m is the mass of the electron with total energy $E = E_\perp + E_\parallel$. $E_\parallel = (\hbar^2/2m)\mathbf{k}_\parallel^2$, where $\mathbf{k}_\parallel$ is the component of the wave vector parallel to the lead-barrier interface. In the leads, $\mu_{R(L)} = \pm eV/2$ and in the spacer, $\mu_S = E_S$, where E_S tunes the Fermi level of the spacer with respect to the leads [see Fig. 1(b)]. In the absence of a voltage drop, $eV = 0$, and therefore the wave functions in the barriers become

$$\Psi_{B_i}^\sigma(y) = a_{B_i}^\sigma \exp(-q_i^\sigma \cdot y) + b_{B_i}^\sigma \exp(q_i^\sigma \cdot y), \tag{4}$$

where $q_i^\sigma = \sqrt{(2m_B/\hbar^2)(U_i - E_\perp - \sigma\Delta_i)}$ is the evanescent wave number. U_i is the height of the ith barrier and m_B is the effective mass of the electron in the barrier. Next, we explicitly calculate the amplitudes associated with the wave functions by matching the wave functions and their derivatives at all interfaces while taking into account the spinor rotation on L and B_1 [60]. The local charge and spin-current densities are calculated considering

$$j_y = \frac{e\hbar}{m} \sum_\sigma \Psi^{\sigma *}(y) \partial_y \Psi^\sigma(y), \tag{5}$$

$$J_y^j = \frac{i\hbar}{2m} \left[\partial_y \Psi^\dagger(y) \sigma_j \Psi(y) - \Psi^\dagger(y) \sigma_j \partial_y \Psi(y) \right], \tag{6}$$

where σ_j, with $j = x$, y, or z, indicates the Pauli components matrix and $\Psi(y) = [\Psi^\uparrow(y), \Psi^\downarrow(y)]^T$ is the wave function of the electron. To calculate the total charge and spin-current densities, we need to take into account the contributions originating from the left and right leads; therefore, considering that the total energy and $\mathbf{k}_\parallel$ are conserved, we have

$$\langle j_y \rangle = \mathrm{Re} \left[\int \left(j_y^{L\to R} f_L + j_y^{R\to L} f_R \right) dE d\mathbf{k}_\parallel \right], \tag{7}$$

$$\langle J_y^j \rangle = \mathrm{Re} \left[\int \left(J_y^{j\,L\to R} f_L + J_y^{j\,R\to L} f_R \right) dE d\mathbf{k}_\parallel \right]. \tag{8}$$

$a^{L\to R(R\to L)}$ is the expectation value of observable a for an electron moving from left to right (right to left). $f_{L(R)} = (1 + e^{(E-\mu_{L(R)}-E_F)/k_B(T_0 \pm \Delta T/2)})^{-1}$ is the Fermi-Dirac distribution for electrons from the left (right). $T_0 = (T_R + T_L)/2$ is the mean temperature, k_B is the Boltzmann constant, and E_F is the Fermi energy. Finally, the net spin-torque components for DMTJs and DSFTJs are derived considering Eqs. (1) and (2), respectively.

B. Tight-binding model

The Hamiltonian considered in the present study is described by the single-orbital simple cubic tight-binding

Hamiltonian in noncollinear configuration, defined as

$$\hat{H} = \hat{H}_L + \hat{H}_{B_1} + \hat{H}_S + \hat{H}_{B_2} + \hat{H}_R + \hat{H}_{\text{int}}, \tag{9}$$

where

$$\hat{H}_\Omega = \sum_{\substack{i \\ (i\in\Omega)}} (\epsilon^0_{\Omega,i}\hat{\mathbf{c}}^\dagger_i\hat{\mathbf{c}}_i + \Delta_\Omega\hat{\mathbf{c}}^\dagger_i\hat{\boldsymbol{\sigma}}\cdot\hat{\mathbf{m}}_\Omega\hat{\mathbf{c}}_i) + \sum_{\substack{i\neq i' \\ (i,i'\in\Omega)}} t\hat{\mathbf{c}}^\dagger_i\hat{\mathbf{c}}_{i'}. \tag{10}$$

Ω represents the uncoupled left (L), right (R), spacer (S), or barrier (B) regions. $\hat{H}_{\text{int}} = t\hat{\mathbf{c}}^\dagger_a\hat{\mathbf{c}}_\alpha + t\hat{\mathbf{c}}^\dagger_b\hat{\mathbf{c}}_{\alpha'} + t\hat{\mathbf{c}}^\dagger_\alpha\hat{\mathbf{c}}_a + t\hat{\mathbf{c}}^\dagger_{\alpha'}\hat{\mathbf{c}}_b$ defines the coupling with the leads. $\hat{\mathbf{c}}^\dagger_i = (c^{\dagger\uparrow}_i, c^{\dagger\downarrow}_i)$, where c^σ_i ($c^{\dagger\sigma}_i$) annihilates (creates) an electron with spin σ on site i ($\in\Omega$). t is the spin-independent hopping parameter between sites restricted to nearest neighbors and is assumed constant everywhere ($t = 1$ eV). In Eq. (10), $\epsilon^0_{\Omega,i} = (\epsilon^\downarrow_{\Omega,i} + \epsilon^\uparrow_{\Omega,i})/2$ represents the averaged on-site energy on atomic layer i, $\Delta_\Omega = (\epsilon^\downarrow_\Omega - \epsilon^\uparrow_\Omega)/2$ is the exchange splitting driven by the magnetization vector, $\hat{\mathbf{m}}_\Omega$, and $\hat{\boldsymbol{\sigma}} = \{\sigma_x, \sigma_y, \sigma_z\}$ is the Pauli matrix vector. In $\hat{H}_{\text{int}}$, subscripts $\alpha(\alpha')$ and $a(b)$ refer to atomic sites near the L/B_1 (B_2/R) interface. Figure 1(a) shows the potential profile where the averaged on-site energies and exchange splittings are described for the particular case of a double-barrier tunnel junction of the form FM/I/NM/I/FM subjected to a thermal difference. We employ the nonequilibrium Green's function technique, where the ferromagnetic leads are treated considering 2×2 semi-infinite Green's functions and the finite region is treated by matrix inversion, i.e., $\hat{g} = \hat{I}/(E - \hat{H}_F)$. $\hat{g}$ represents the Green's function matrix, $\hat{I}$ is the identity matrix, and $\hat{H}_F$ is the Hamiltonian of the finite region, given by $B_1/S/B_2$. In this work, we consider $N_B = 2$, N_B being the number of atomic sites in each barrier. The system is then coupled through Dyson's equation [61],

$$\hat{G}_{pq} = \hat{g}_{pq} + \hat{g}_{pa}\hat{\Sigma}_{aa}\hat{G}_{aq} + \hat{g}_{pb}\hat{\Sigma}_{bb}\hat{G}_{bq}, \tag{11}$$

where $\hat{G}(\hat{g})$ is the 2×2 coupled (isolated) retarded Green's function matrix, subscripts p and q denote atomic sites in the finite region, and the self-energy terms given by $\hat{\Sigma}_{aa(bb)} = t^2\hat{g}_{\alpha\alpha(\alpha'\alpha')}$ take into account the propagation of the electron across the barrier-leads interfaces. Equation (11) is self-consistently solved and analytical expressions for the coupled retarded Green's functions, $\hat{G}_{pq}$, are obtained. To evaluate the local spin-current and charge-current densities, we proceed to solve the quantum kinetic equation based on Keldysh formalism, which yields solutions for the 2×2 lesser Green's functions, $\hat{G}^<$ [61]. Consequently, we have

$$\langle j_{p,p+1}\rangle = \frac{e}{h}\frac{t}{4\pi^2}\text{Re}\left[\int \text{Tr}[(\hat{G}^<_{p+1,p} - \hat{G}^<_{p,p+1})\cdot\hat{I}]dEd\mathbf{k}_\parallel\right], \tag{12}$$

$$\langle J^j_{p,p+1}\rangle = \frac{t}{16\pi^3}\text{Re}\left[\int \text{Tr}[(\hat{G}^<_{p+1,p} - \hat{G}^<_{p,p+1})\cdot\hat{\sigma}_j]dEd\mathbf{k}_\parallel\right], \tag{13}$$

where e is the electric charge, h is Planck's constant, and $\mathbf{k}_\parallel$ is the transverse component of the wave vector. Finally, the local spin torque at position i is calculated considering $T_i = \langle J_{i-1,i}\rangle - \langle J_{i,i+1}\rangle$, which reduces to the net spin-torque components given in Eqs. (1) and (2).

III. ANALYTICAL RESULTS

In this section, we present our analytical results of the thermocurrent and the thermal spin-current densities in two types of double-barrier tunnel junctions considered in this work: (i) FM/I/S/I/FM and (ii) NM/FI/S/FI/NM. We use Sommerfeld expansion to obtain a qualitative understanding of the temperature and energy dependence of the observables and then we study the thick- and/or large-barrier regime to understand the underlying mechanism of the spin-torque amplitudes.

A. Sommerfeld expansion

For symmetric junctions, the operators for the charge-current and the in-plane spin-current densities are antisymmetric, i.e., $j_y^{(L\to R)} = -j_y^{(R\to L)}$ and $J_y^{x,z(L\to R)} = -J_y^{x,z(R\to L)}$, while that for the out-of-plane spin-current density is symmetric, i.e., $J_y^{y(L\to R)} = J_y^{y(R\to L)}$. From this observation, a straightforward application of Sommerfeld expansion reveals that for symmetric junctions subjected to a temperature difference, the charge and spin-current densities are given by

$$\langle j_y\rangle \approx \xi(T_0\Delta T)\int dE_\parallel \partial_E j_y(E_F - E_\parallel), \tag{14}$$

$$\langle J^y_y\rangle \approx \xi(T_0^2 + \tfrac{1}{4}\Delta T^2)\int dE_\parallel \partial_E J^y_y(E_F - E_\parallel), \tag{15}$$

$$\langle J^{x,z}_y\rangle \approx \xi(T_0\Delta T)\int dE_\parallel \partial_E J^{x,z}_y(E_F - E_\parallel), \tag{16}$$

where $\xi = m^2k_B^2/12\hbar^4$. These equations show that the thermally driven spin-current density exhibits the same symmetry against bias as its electrically driven counterpart, i.e., the in-plane spin-current density is *antisymmetric* against the thermal gradient ($\propto T_0\Delta T$), whereas the out-of-plane spin-current density is *symmetric* ($\propto T_0^2 + \frac{1}{4}\Delta T^2$). Moreover, (i) the efficiency of the in-plane spin-current density increases linearly with the sample temperature

and (ii) the out-of-plane spin-current density is dominated by the thermal contribution rather than the thermal gradient ($T_0^2 \gg \Delta T^2$). Consequently, the zero-bias interlayer exchange coupling, $J_y^y(\Delta T = 0)$, is enhanced due to the thermally activated enhancement of the tunneling electrons and therefore the net spin torque in the absence of $J_y^y(\Delta T = 0)$ is dominated by the in-plane spin-current contribution. Note that this thermal dependence has nothing to do with the band structure, since both T_0 and ΔT are very small compared to the Fermi energy. In the presence of finite ferromagnetic barriers, the contributions from left to right and right to left are not the same; therefore, as noted in the following section, the thermal dependence given by Sommerfeld expansion is not valid; as a result, the out-of-plane component is no longer symmetric and its magnitude becomes comparable to that of the in-plane component due to the spin-filtering effect. For ferromagnetic leads attached to nonmagnetic barriers, in order to obtain a perpendicular component much larger than the in-plane component, one needs to tune the interface resonant states so that $\partial_E J_y^y(E_F - E_\parallel)/\partial_E J_y^x(E_F - E_\parallel) \gg T_0/\Delta T \approx 10^2$; consequently, the previous work of Jia *et al.* [19] that has computed a much larger perpendicular thermal torque compared to the in-plane component in conventional MTJs has to be revisited in light of the results presented here.

B. Thick- and/or large-barrier regime

1. Double magnetic tunnel junction

In systems of the form FM/I/S/I/FM with identical barriers, the charge-current density for electrons moving from left to right ($L \to R$) reads

$$j_y^{(L\to R)} = \frac{e\hbar}{m}\gamma_S j_0\,(1 + \mathcal{P}_L\mathcal{P}_R\cos\theta)\,e^{-2qd}, \tag{17}$$

where $d = d_{B_1} + d_{B_2}$, d_{B_i} being the barrier thickness,

$$j_0 = \frac{16\kappa^4(\kappa^2 + k_L^\uparrow k_L^\downarrow)(k_L^\uparrow + k_L^\downarrow)(\kappa^2 + k_R^\uparrow k_R^\downarrow)(k_R^\uparrow + k_R^\downarrow)}{(\kappa^2 + k_L^{\downarrow 2})(\kappa^2 + k_L^{\uparrow 2})(\kappa^2 + k_R^{\downarrow 2})(\kappa^2 + k_R^{\uparrow 2})}, \tag{18}$$

and

$$\mathcal{P}_\nu = \frac{k_\nu^\uparrow - k_\nu^\downarrow}{k_\nu^\uparrow + k_\nu^\downarrow}\frac{\kappa^2 - k_\nu^\uparrow k_\nu^\downarrow}{\kappa^2 + k_\nu^\uparrow k_\nu^\downarrow}. \tag{19}$$

$\mathcal{P}_\nu$ is the polarization of the νth lead and $\kappa = qm/m_B$. γ_S is the Lorentzian function that captures all the important physics of resonant tunneling and is given by

$$\gamma_S = \left(\frac{k_S}{\kappa^2 + k_S^2}\frac{1}{\sin(k_S d_S + \phi)}\right)^2, \tag{20}$$

where $\phi = \tan^{-1}\left[2k_S\kappa/(\kappa^2 - k_S^2)\right]$. In the absence of the metallic spacer, its thickness $d_S = 0$ and $\gamma_S = 1$. This reduces the system to the conventional single-barrier MTJ with barrier thickness d [60,62]. In the presence of the metallic spacer, Eq. (20), which represents a significant finding of this work, reveals that the broadening, the period, and the position of the resonant peaks are determined by $k_S/(\kappa^2 + k_S^2)$, $\sin(k_S d_S + \phi)$, and ϕ, respectively. Therefore, it is possible to tune the resonant peaks in different samples through efficient material engineering, such as varying the spacer thickness or its energy. We now consider the solutions for the spin-current density components at the $B_2|R$ interface:

$$J_{y_r}^{x(L\to R)} = \frac{\hbar^2}{2m}\gamma_S j_0 \mathcal{P}_L \sin\theta e^{-2qd}, \tag{21}$$

$$J_{y_r}^{y(L\to R)} = \frac{\hbar^2}{2m}\gamma_S j_0 \frac{\kappa(k_R^\downarrow - k_R^\uparrow)}{\kappa^2 + k_R^\downarrow k_R^\uparrow}\mathcal{P}_L \sin\theta e^{-2qd}, \tag{22}$$

$$J_{y_r}^{z(L\to R)} = \frac{\hbar^2}{2m}\gamma_S j_0\,(\mathcal{P}_R + \mathcal{P}_L\cos\theta)\,e^{-2qd}. \tag{23}$$

As shown in Eqs. (21) and (22), the ratio $J_{y_r}^x/J_{y_r}^y$ is proportional to $(\kappa^2 + k_R^\downarrow k_R^\uparrow)/\kappa(k_R^\downarrow - k_R^\uparrow)$, suggesting that the x component of the spin-current density exhibits a larger amplitude than the y component. It is important to note that the information about the spin-current density along the quantization axis, $J_{y_r}^z$, gives complete information about the in-plane spin-current density, i.e.,

$$\frac{1}{2}[J_{y_r}^z(\theta = 0) - J_{y_r}^z(\theta = \pi)]\sin\theta = J_{y_r}^x. \tag{24}$$

Equation (24) represents the generalization of the results given for single-barrier MTJs in Refs. [57–59,62]. The results for electrons moving from right to left ($R \to L$) can be obtained from the above expressions by symmetry arguments. Finally, the spin-torque components are calculated considering Eq. (1).

2. Double-spin-filter tunnel junction

In contrast to DMTJs, where the three components of the spin-current density are proportional to e^{-2qd}, in systems of the form NM/FI/S/FI/NM, the y component of the spin-current density is proportional to the order in the barrier transmission, $e^{-q^\sigma d}$, whereas the other two components are proportional to $e^{-2q^\sigma d}$. These results suggest that in double-barrier spin-filter tunnel junctions, the out-of-plane component of the thermal spin torque is much larger than in DMTJs. To understand this, we consider the limit of identical barriers and obtain

$$J_{y_s}^{y(L\to R)} = \frac{2\hbar^2}{m}\sum_\sigma \sigma\frac{\gamma_L^\sigma k_L \kappa^{\sigma 2}(\kappa^\downarrow - \kappa^\uparrow)}{k_L^2 + \kappa^{\sigma 2}}\sin\theta e^{-q^\sigma d}, \tag{25}$$

$$J_{y_s}^{y(R\to L)} = \frac{2\hbar^2}{m}\sum_{\sigma}\sigma\frac{\gamma_L^{\sigma}k_R\kappa^{\sigma 2}(\kappa^{\downarrow}-\kappa^{\uparrow})}{k_R^2+\kappa^{\sigma 2}}\sin\theta e^{-q^{\sigma}d}, \tag{26}$$

and

$$J_{y_r}^{y(L\to R)} = J_{y_s}^{y(L\to R)}e^{-d(q^{\uparrow}+q^{\downarrow})/2}, \tag{27}$$

$$J_{y_r}^{y(R\to L)} \approx \frac{\hbar^2}{m}\gamma_R\mathcal{P}_B k_R(\kappa^{\downarrow}-\kappa^{\uparrow})\sin\theta e^{-d(q^{\uparrow}+q^{\downarrow})/2}. \tag{28}$$

$\mathcal{P}_B = [(\kappa^{\downarrow 2}-\kappa^{\uparrow 2})(\kappa^{\downarrow}\kappa^{\uparrow}-k_R^2)]/[(\kappa^{\downarrow 2}+k_R^2)(\kappa^{\uparrow 2}+k_R^2)]$ and $\gamma_{L(R)}^{\sigma}$ is defined in Ref. [63], which reduces to Eq. (20) when $\kappa^{\uparrow}=\kappa^{\downarrow}$, i.e., $\lim_{\Delta_B\to 0}\gamma_{L(R)}^{\sigma}=\gamma_S$. The above expressions show that electrons not tunneling through both barriers give rise to lower-order contributions that are not present in DMTJs. Moreover, whereas Eqs. (25) and (26) show a symmetric contribution to the torque at the $S|B_2$ interface, Eqs. (27) and (28) show, in contrast, a nonsymmetric contribution at the second interface that is driven by the spin-dependent reflection of the electrons flowing from right to left.

IV. NUMERICAL RESULTS

In this section, we present our numerical results of the thermal spin-torque components in double-barrier tunnel junctions having the general form $L/B_1/S/B_2/R$. Previously, we have shown analytically that the amplitude of the perpendicular spin-current density in systems made of nonmagnetic leads in contact with magnetic barriers (DSFTJs) is expected to be much larger than in systems made of ferromagnetic leads in contact with nonmagnetic barriers (DMTJs). Moreover, the latter are shown to have a net spin torque dominated by the in-plane component. Here, we exploit the numerical advantages to perform systematic studies of the thermal spin-torque components as a function of the spacer thickness and the thermal difference. We address the tight-binding results for two regimes. In one case, we consider ferromagnetic materials with low exchange-splitting values, $\Delta = 0.5$ eV; this is referred to, in the present work, as the low-band-filling (LB) regime. In the second case, we consider ferromagnetic samples where the contribution to the transport of minority carriers is negligible. In ferromagnetic metals, this is called a half-metallic system, whereas in magnetic insulators, this gives rise to an idealized spin-filtering effect with 100% spin polarization. For simplicity, we term this second case the one-band-filling (OB) regime and consider an exchange splitting of $\Delta = 1.5$ eV. We then study the free-electron model to capture the spacer thickness dependence for different values of E_S. In Fig. 2, we present the former results, where we describe the thermal spin-torque components for DMTJ and DSFTJ structures as a function of the thermal difference. For the perpendicular component, the zero-bias contribution, $T_{\perp}^0$, is subtracted. In both systems, similar parameters are considered, as noted in the caption of Fig. 2. As shown, DSFTJ structures exhibit larger torque amplitudes compared to DMTJs. In particular, for similar parameters of the exchange splitting, $T_{\perp}-T_{\perp}^0$ in DSFTJs can be 3 orders of magnitude larger than in DMTJs. This result is understood considering Eqs. (22) and (25), where we have $T_{\perp}(\text{DMTJ}) \propto e^{-2qd} \ll T_{\perp}(\text{DSFTJ}) \propto e^{-q^{\sigma}d}$. In terms of the torque efficiencies, denoted by $T_{\perp}-T_{\perp}^0/j_y$, these results remain unchanged [see the inset in Fig. 2(b)]. It is important to remark upon the behavior of $T_{\parallel}$ and $T_{\perp}-T_{\perp}^0$ as a function of ΔT. $T_{\parallel}$ exhibits monotonic behavior. In DSFTJs, it has the same symmetry for both regimes, LB and OB; however, in DMTJs, for a given thermal difference sign, it changes sign for each regime [see Fig. 2(a)]. This behavior is understood considering single-barrier junctions and has been explained in Ref. [53]. There, the authors have shown that in MTJs the sign of $T_{\parallel}$

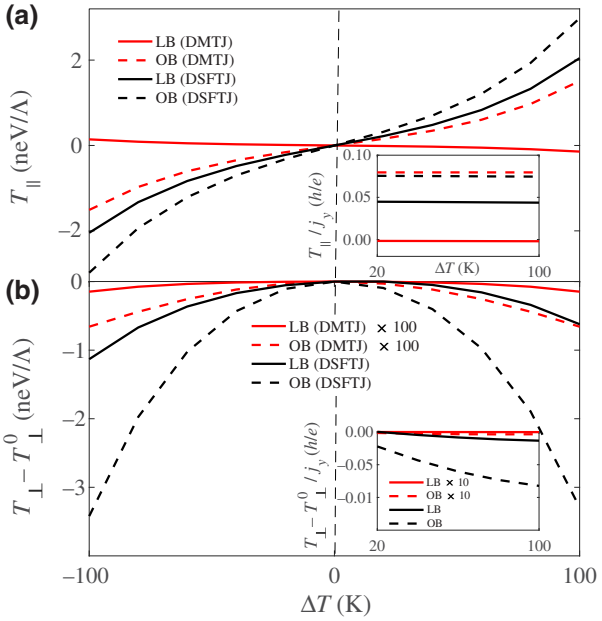

FIG. 2. The thermal dependence of the nonequilibrium (a) in-plane, $T_{\parallel}$, and (b) out-of-plane, $T_{\perp}-T_{\perp}^0$, spin-torque components for DMTJ (red) and DSFTJ (black) structures in units of neV/Λ, where Λ denotes the interfacial unit area. The relative angle of the magnetic vectors is set to $\theta = \pi/2$ and the mean temperature is $T_0 = 300$ K. The insets refer to the spin-torque efficiencies in units of h/e. In DMTJs, we have $\epsilon_B^{\uparrow(\downarrow)} = 7$ eV and then (i) for LB, $\epsilon_{L,R}^{\uparrow(\downarrow)} = 4(5)$ eV and (ii) for OB, $\epsilon_{L,R}^{\uparrow(\downarrow)} = 4(7)$ eV. In DSFTJs, we have $\epsilon_{L,R}^{\uparrow(\downarrow)} = 4$ eV and then (i) for LB, $\epsilon_B^{\uparrow(\downarrow)} = 7(8)$ eV and (ii) for OB, $\epsilon_B^{\uparrow(\downarrow)} = 7(10)$ eV. In all cases, $\epsilon_S^{\uparrow(\downarrow)} = 5$ eV. Note that in both systems the LB regime is defined considering $\Delta = 0.5$ eV, whereas the OB regime is defined considering a larger exchange splitting ($\Delta = 1.5$ eV). In (b), the torque amplitudes and the torque efficiencies for DMTJs are multiplied by 100 and 10, respectively, to fit into the graph.

is determined by the polarization factor, whereas in SFTJs no sign reversal is expected as a result of the spin-filtering effect. $T_\perp - T_\perp^0$, in contrast, becomes an even function in DMTJs but is nonsymmetric in DSFTJs [see Fig. 2(b)]. This is understood considering Eqs. (27) and (28), where we show that a finite magnetic insulating barrier breaks the symmetry due to a greater contribution from the spin-dependent reflection. Overall, our results show that for similar parameters, the electronic transport in DSFTJs gives rise to a greater thermal torque efficiency compared to DMTJs. Note, however, that the in-plane component, $T_\parallel/j_y$, is comparable in magnitude for both types of systems in the OB regime. Moreover, if we decrease the exchange splitting in the ferromagnetic barriers (from OB to LB), the spin-torque amplitudes in DSFTJs remain larger than in DMTJs, even if the latter preserves a large splitting value in the half-metallic regime (OB), suggesting that conventional ferromagnetic insulators with low exchange, such as Eu chalcogenides or spinel-based materials, may give rise to thermal torques that are larger than in DMTJs. Whereas the in-plane torque dominates in DMTJs, in DSFTJs, both components, in-plane and out-of-plane, are comparable in magnitude and therefore $T_\perp$ cannot be neglected. In DSFTJs, a more realistic device may require a ferromagnetic metal to couple one magnetic insulator. Although not shown here, inclusion of a ferromagnetic metal in a DSFTJ structure enhances the torque amplitudes; however, this enhancement is minimal, as the driven mechanism of the tunneling process is the spin filtering in the barriers. We now proceed to study the thermal spin-torque efficiencies as a function of the spacer thickness for different values of E_S. Instead of using the discretized tight-binding model, we consider the free-electron model to better capture the resonance-tunneling mechanism, which is driven by Eq. (20) in DMTJs and Ref. [63] in DSFTJs. We take into account realistic parameters as stated in Refs. [54] and [55], i.e., our DSFTJ system considers EuO-like ferromagnetic barriers with an exchange splitting of 0.5 eV, whereas the DMTJ structure is adjusted to resemble Fe/MgO MTJs with an exchange splitting of 1.96 eV. The former is the usual DSFTJ in the LB regime discussed with the tight-binding model. The latter is also in the same regime but with a larger exchange splitting and therefore the spin-torque amplitudes are expected to be smaller than those of a half-metallic system but larger than those of the LB system discussed previously. It is important to note that the free-electron model, properly speaking, does not describe a ferromagnetic insulator, because in this case the ferromagnetism in, for example, EuO arises from the $4f$ localized states and therefore a multiband analysis is required [64]. However, in the context of the transport modeling, highly conductive itinerant electrons are mainly s-d spin-polarized and therefore focusing on these bands above the Fermi level in the insulating region is a good approximation from a qualitative standpoint [43–45]. For

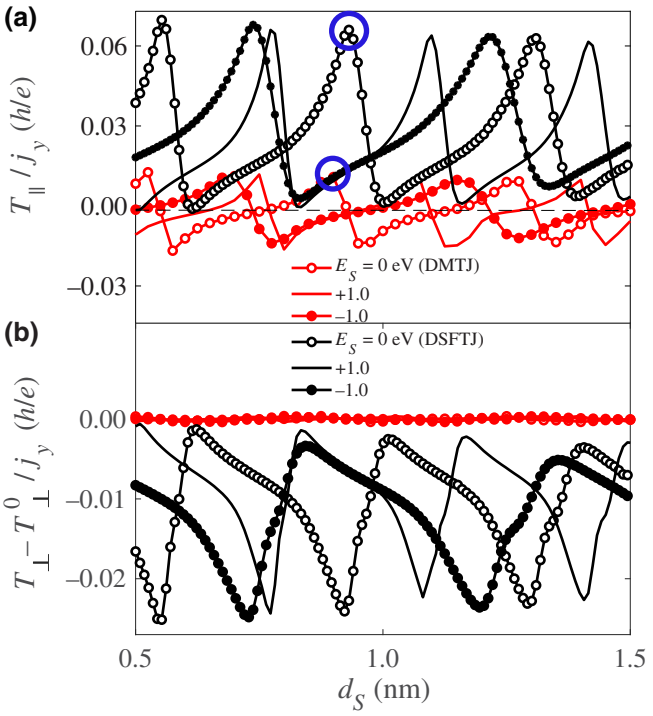

FIG. 3. The spacer-thickness dependence of the nonequilibrium (a) in-plane, $T_\parallel/j_y$, and (b) out-of-plane, $(T_\perp - T_\perp^0)/j_y$, thermal spin-torque efficiencies in units of h/e for DMTJ (red) and DSFTJ (black) structures. Three values of E_S are considered; 0, 1.0, and -1.0 eV. The relative angle of the magnetic vectors is set to $\theta = \pi/2$. $E_F = 2.62$ eV, $U = E_F + 0.8$ eV, $m = 9.1 \times 10^{-31}$ kg, $m_B = 0.4$ m, $\Delta T = 50$ K, and $T_0 = 300$ K. In DMTJs, $\Delta = 1.96$ eV, and in DSFTJs, $\Delta = 0.5$ eV. The blue circles in the upper panel denote the case $E_S = 0$ eV and $d_S \sim 0.9$ nm.

simplicity, the thermal spin-torque components are calculated considering the relative orientation of the magnetic vectors to be perpendicular to each other. Note, however, that in DSFTJs, $\gamma^\sigma_{L(R)}$ also depends on θ; therefore, in such systems, the maximum values of the torques are slightly shifted from $\theta = \pi/2$. In Fig. 3, we are more interested in studying the relative differences between DMTJs and DSFTJs. As shown, due to the quantum resonance, the in-plane and the out-of-plane thermal spin-torque efficiencies can be, respectively, one order and 3 orders of magnitude larger in DSFTJs than in DMTJs. Note that in Fig. 2, a similar conclusion is obtained when comparing systems with similar exchange-splitting values. In this case, we show that even if we take a much smaller exchange value in DSFTJs, due to the presence of quantum resonance, one can obtain larger thermal spin-torque efficiencies when considering ferromagnetic insulators. An important feature in DMTJs is that these efficiencies change sign as we tune d_S or E_S. In contrast, in DSFTJs the efficiencies do not experience a sign reversal as a result of the spin-filtering process. To connect these results to experiments, in Table I we compare our double-barrier systems with a

single-barrier MTJ used for spin-transfer-torque magnetic random-access memory (STT MRAM) applications. In particular, we choose double-barrier junctions with $E_S = 0$ eV and $d_S \sim 0.9$ nm, which correspond, for the parameters given here, to the largest in-plane torque efficiencies [see Fig. 3(a), blue circles]. The single-barrier MTJ is chosen with parameters similar to the DMTJ. In all cases, we keep the same barrier width, i.e., $d_B = d_{B_1} = d_{B_2} = 0.5$ nm, where d_B is the barrier width of the MTJ. As noted in Ref. [24], an in-plane torque of 0.02 μeV/Å^2 can be sufficient to induce switching of the storage-layer magnetization. This is possible in single-barrier MTJs considering a voltage drop that gives rise to a pure charge-current density on the order of $10^5 - 10^6$ A/cm^2 (see Table I, first row). However, when considering instead a thermal difference that gives rise to an equivalent charge-current density, the thermal torque generated is small and not enough for data-storage applications (see Table I, second row). Note that these results depend strongly on the parameters chosen, and in this case one may expect that thermal torques are not suitable to replace spin-transfer torques. Nonetheless, if we take into account double-barrier junctions and keep the same thermal difference, we obtain a dramatic enhancement of the spin-torque amplitude (see Table I, third and fourth rows). In particular, the in-plane thermal spin torque in DSFTJs can be one order of magnitude larger than the amplitude needed for magnetization switching, suggesting that DSFTJ structures are more efficient than MTJs. To better quantify this efficiency, in thermal systems, we should be interested in minimizing the heat current while maximizing the Seebeck coefficient. To minimize the heat current, lower temperatures or larger effective masses can be considered [65]. In DSFTJs, due to a larger spin-torque amplitude, lowering the mean temperature of the system, for example, would still give rise to spin torques that are sufficient for magnetization switching, which is not the case when considering DMTJs or MTJs (see Table I). Therefore, DSFTJs offer a better flexibility for tuning parameters in data-storage applications. Regarding the Seebeck coefficient, in Ref. [66] the author has shown that in DSFTJ structures, this coefficient increases by 2 orders of magnitude compared to single-barrier MTJs. Although in this work we use different parameters, due to the resonant states present in the system, a similar enhancement is expected. Consequently, our results suggest a larger figure of merit in DSFTJ structures compared to DMTJs and single-barrier MTJs. However, it is important to note that the contribution to the thermal conductance is made not only by electrons but also by phonons, and therefore in systems where the heat transport by phonons is important, the figure of merit decreases. In this sense, further studies to quantify these contributions are needed, as has been done in Ref. [67] for half-MTJs. Nonetheless, in heterostructures composed of different materials, the transport of heat by phonons is partially blocked and we expect that this contribution will not be significant.

TABLE I. Typical values of the charge current density, in-plane torque, and the in-plane torque efficiency for an MTJ, DMTJ, and DSFTJ subjected to a temperature difference of 50 K compared to a reference system of an MTJ subjected to an equivalent voltage drop of 0.886 meV. In all cases, the barrier width is set at 0.5 nm, $E_S = 0$ eV, and $d_S = 0.9$ nm, while all other parameters are the same as in Fig. 3.

System	j_e (A/cm^2)	$T_\parallel$ (μeV/Å^2)	$T_\parallel/j_e$ (h/e)
MTJ (0.886 meV)	0.5×10^6	0.038	~ 0.03
MTJ (50 K)	0.5×10^6	0.003	~ 0.002
DMTJ (50 K)	0.6×10^6	0.017	~ 0.01
DSFTJ (50 K)	1.0×10^6	0.17	~ 0.06

V. CONCLUSIONS

In this work, we have shown that double-barrier tunnel junctions in the presence of magnetic insulators (DSFTJs) offer an enhanced thermal spin-torque efficiency compared to DMTJs for reliable applications. For the parameters chosen, related to realistic samples used in experimental measurements, such as EuO-based spin-filter tunnel junctions and Fe/MgO-based MTJs, the in-plane and out-of-plane components of the thermal spin-torque efficiency become, respectively, one order and 3 orders of magnitude larger in DSFTJs. Moreover, as a result of the quantum resonance in the system, these values are tuned by either varying the thickness of the spacer or its energy relative to the leads. The latter approach may be used efficiently considering impurity doping [68]. Whereas in DMTJs, the out-of-plane component of the thermal spin torque can be neglected, in DSFTJs, both components, in-plane and out-of-plane, are comparable in magnitude. We also study a half-metallic DMTJ structure and show that even when considering this type of system, the amplitude of the thermal spin torque remains larger in DSFTJs and this difference keeps increasing as one increases the exchange splitting in the ferromagnetic barriers. Finally, we have shown that the in-plane torque amplitude in DSFTJs can reach values that are one order of magnitude larger than the amplitude needed for magnetization switching. Considering the recent progress in observation of quantum resonant tunneling in magnetic tunnel junctions with two or more barriers [69,70], these findings may open up avenues for exploring various kinds of ferromagnetic insulators with larger exchange splittings and higher transition temperatures, which can lead to more efficient devices in the absence of external currents.

ACKNOWLEDGMENTS

C.O.P. and C.A.A. thank, respectively, S. Nikolaev and A. Manchon for useful discussions. This work was

supported by a Grant-in-Aid for Exploratory Research (Grant No. 16K13853) and a Grant-in-Aid for Scientific Research (B) (Grant No. 17H02929) from the Japan Society for the Promotion of Science (JSPS).

[1] G. E. W. Bauer, E. Saitoh, and B. J. van Wees, Spin caloritronics, Nat. Mater. **11**, 391 (2012).
[2] K. Uchida, S. Takahashi, K. Harii, J. Ieda, W. Koshibae, K. Ando, S. Maekawa, and E. Saitoh, Observation of the spin Seebeck effect, Nature **455**, 778 (2008).
[3] A. Slachter, F. L. Bakker, J. P. Adam, and B. J. van Wees, Thermally driven spin injection from a ferromagnet into a non-magnetic metal, Nat. Phys. **6**, 879 (2010).
[4] K. Uchida, T. Ota, K. Harii, S. Takahashi, S. Maekawa, Y. Fujikawa, and E. Saitoh, Spin-Seebeck effects in $Ni_{81}Fe_{19}$/Pt films, Solid State Commun. **150**, 524 (2010).
[5] K. Uchida, J. Xiao, H. Adachi, J. Ohe, S. Takahashi, J. Ieda, T. Ota, Y. Kajiwara, H. Umezawa, H. Kawai, G. E. W. Bauer, S. Maekawa, and E. Saitoh, Spin Seebeck insulator, Nat. Mater. **9**, 894 (2010).
[6] C. M. Jaworski, J. Yang, S. Mack, D. D. Awschalom, J. P. Heremans, and R. C. Myers, Observation of the spin-Seebeck effect in a ferromagnetic semiconductor, Nat. Mater. **9**, 898 (2010).
[7] S. Bosu, Y. Sakuraba, K. Uchida, K. Saito, T. Ota, E. Saitoh, and K. Takanashi, Spin Seebeck effect in thin films of the Heusler compound Co_2MnSi, Phys. Rev. B **83**, 224401 (2011).
[8] J. Xiao, G. E. W. Bauer, K. C. Uchida, E. Saitoh, and S. Maekawa, Theory of magnon-driven spin Seebeck effect, Phys. Rev. B **81**, 214418 (2010).
[9] S. A. Bender and Y. Tserkovnyak, Thermally driven spin torques in layered magnetic insulators, Phys. Rev. B **93**, 064418 (2016).
[10] J. C. Le Breton, S. Sharma, H. Saito, S. Yuasa, and R. Jansen, Thermal spin current from a ferromagnet to silicon by Seebeck spin tunnelling, Nature **475**, 82 (2011).
[11] M. Hatami, G. E. W. Bauer, Q. F. Zhang, and P. J. Kelly, Thermoelectric Effects in Magnetic Nanostructures, Phys. Rev. Lett. **79**, 174426 (2009).
[12] L. Gravier, S. Serrano-Guisan, F. Reuse, and J. P. Ansermet, Thermodynamic description of heat and spin transport in magnetic nanostructures, Phys. Rev. B **73**, 024419 (2006).
[13] M. Czerner, M. Bachmann, and C. Heiliger, Spin caloritronics in magnetic tunnel junctions: *Ab initio* studies, Phys. Rev. B **83**, 132405 (2011).
[14] D. C. Ralph and M. D. Stiles, Spin transfer torques, J. Magn. Magn. Mater. **320**, 1190 (2008).
[15] M. Hatami, G. E. W. Bauer, Q. Zhang, and P. J. Kelly, Thermal Spin-Transfer Torque in Magnetoelectronic Devices, Phys. Rev. Lett. **99**, 066603 (2007).
[16] H. Yu, S. Granville, D. P. Yu, and J.-Ph. Ansermet, Evidence for Thermal Spin-Transfer Torque, Phys. Rev. Lett. **104**, 146601 (2010).
[17] L. Fitoussi, F. A. Vetro, C. Caspers, L. Gravier, H. Yu, and J.-P. Ansermet, Linear response to a heat-driven spin torque, Appl. Phys. Lett. **106**, 162401 (2015).
[18] Z. Yuan, S. Wang, and K. Xia, Thermal spin-transfer torques on magnetic domain walls, Solid State Commun. **150**, 548 (2010).
[19] X. Jia, K. Xia, and G. E. W. Bauer, Thermal Spin Transfer in Fe-MgO-Fe Tunnel Junctions, Phys. Rev. Lett. **107**, 176603 (2011).
[20] A. Pushp, T. Phung, C. Rettner, B. P. Hughes, S.-H. Yang, and S. S. P. Parkin, Giant thermal spin-torque-assisted magnetic tunnel junction switching, Proc. Natl. Acad. Sci. U.S.A. **112**, 6585 (2015).
[21] Z. Zhang, L. Bai, X. Chen, H. Guo, X. L. Fan, D. S. Xue, D. Houssameddine, and C.-M. Hu, Observation of thermal spin-transfer torque via ferromagnetic resonance in magnetic tunnel junctions, Phys. Rev. B **94**, 064414 (2016).
[22] P. Ogrodnik, G. E. W. Bauer, and K. Xia, Thermally induced dynamics in ultrathin magnetic tunnel junctions, Phys. Rev. B **88**, 024406 (2013).
[23] C. Heiliger, C. Franz, and M. Czerner, Thermal spin-transfer torque in magnetic tunnel junctions, J. Appl. Phys. **115**, 172614 (2014).
[24] B. Dieny, M. Chshiev, B. Charles, N. Strelkov, A. Truong, O. Fruchart, A. Hallal, J. Wang, Y. K. Takahashi, T. Mizuno, and K. Hono, Impact of intergrain spin-transfer torques due to huge thermal gradients in heat-assisted magnetic recording, IEEE Trans. Magn. **54**, 12 (2018).
[25] J. A. Stroscio, D. T. Pierce, A. Davies, R. J. Celotta, and M. Weinert, Tunneling Spectroscopy of bcc (001) Surface States, Phys. Rev. Lett. **75**, 2960 (1995).
[26] O. Wunnicke, N. Papanikolaou, R. Zeller, P. H. Dederichs, V. Drchal, and J. Kudrnovsky, Effects of resonant interface states on tunneling magnetoresistance, Phys. Rev. B **65**, 064425 (1995).
[27] S.-Z. Wang, K. Xia, and G. E. W. Bauer, Thermoelectricity and disorder of FeCo/MgO/FeCo magnetic tunnel junctions, Phys. Rev. B **90**, 224406 (2014).
[28] I. Theodonis, A. Kalitsov, and N. Kioussis, Spin transfer torque in double barrier magnetic tunnel junctions, J. Magn. Magn. Mater. **310**, 2043 (2007).
[29] C. H. Chen, Y. H. Cheng, C. W. Ko, and W. J. Hsueh, Enhanced spin-torque in double tunnel junctions using a nonmagnetic-metal spacer, Appl. Phys. Lett. **107**, 152401 (2015).
[30] C. H. Chen, P. Tseng, Y. Y. Yang, and W. J. Hsueh, Enhancement of thermal spin transfer torque by double-barrier magnetic tunnel junctions with a nonmagnetic metal spacer, J. Phys.: Condens. Matter **29**, 025806 (2017).
[31] R. Daqiq, Temperature gradient effects on spin torque in double barrier magnetic tunnel junctions with a non-magnetic metal spacer, J. Supercond. Nov. Magn. **30**, 1593 (2017).
[32] X. Jia, S. Wang, and M. Qin, Enhanced thermal spin transfer in MgO-based double-barrier tunnel junctions, New J. Phys. **18**, 063012 (2016).
[33] H. Wu, L. Huang, C. Fang, B. S. Yang, C. H. Wan, G. Q. Yu, J. F. Feng, H. X. Wei, and X. F. Han, Magnon Valve Effect between Two Magnetic Insulators, Phys. Rev. Lett. **120**, 097205 (2018).
[34] C. Y. Guo, C. H. Wan, X. Wang, C. Fang, P. Tang, W. J. Kong, M. K. Zhao, L. N. Jiang, B. S. Tao, G. Q. Yu, and X. F. Han, Mangon valves based on YIG/NiO/YIG

all-insulating magnon junctions, Phys. Rev. B **98**, 134426 (2018).
[35] L. J. Cornelissen, J. Liu, R. A. Duine, J. B. Youssef, and B. J. van Wees, Long-distance transport of mangon spin information in a magnetic insulator at room temperature, Nat. Phys. **11**, 1022 (2015).
[36] Y. Cheng, K. Chen, and S. Zhang, Giant magneto-spin-Seebeck effect and magnon transfer torques in insulating spin valves, Appl. Phys. Lett. **112**, 052405 (2018).
[37] D. Hinzke and U. Nowak, Domain Wall Motion by the Magnonic Spin Seebeck Effect, Phys. Rev. Lett. **107**, 027205 (2011).
[38] P. Yan, X. S. Wang, and X. R. Wang, All-Magnonic Spin-Transfer Torque and Domain Wall Propagation, Phys. Rev. Lett. **107**, 177207 (2011).
[39] Y. Cheng, W. Wang, and S. Zhang, Amplification of spin-transfer torque in magnetic tunnel junctions with an antiferromagnetic barrier, Phys. Rev. B **99**, 104417 (2019).
[40] R. Cheng, D. Xiao, and J.-G. Zhu, Antiferromagnet-based magnonic spin-transfer torque, Phys. Rev. B **98**, 020408(R) (2018).
[41] H.-M. Tang, X.-T. Jia, and S.-Z Wang, Thermal spin transfer torque in Fe/Ag/YIG multilayers, Front. Phys. **12**, 128501 (2017).
[42] J. C. Slonczewski, Initiation of spin-transfer torque by thermal transport from magnons, Phys. Rev. B **82**, 054403 (2010).
[43] G.-X. Miao, M. Muller, and J. S. Moodera, Magnetoresistance in Double Spin Filter Tunnel Junctions with Nonmagnetic Electrodes and Its Unconventional Bias Dependence, Phys. Rev. Lett. **102**, 076601 (2009).
[44] J. S. Moodera, R. Merservey, and X. Hao, Variation of the Electron-Spin Polarization in EuSe Tunnel Junctions from Zero to Near 100% in a Magnetic Field, Phys. Rev. Lett. **70**, 853 (1993).
[45] T. S. Santos and J. S. Moodera, Observation of spin filtering with a ferromagnetic EuO tunnel barrier, Phys. Rev. B **69**, 241203(R) (2004).
[46] M. G. Chapline and S. X. Wang, Room-temperature spin filtering in a $CoFe_2O_4/MgAl_2O_4/Fe_3O_4$ magnetic tunnel barrier, Phys. Rev. B **74**, 014418 (2006).
[47] U. Luders, M. Bibes, S. Fusil, K. Bouzehouane, E. Jacquet, C. B. Sommers, J.-P. Contour, J.-F. Bobo, A. Barthélémy, A. Fert, and P. M. Levy, Bias dependence of tunnel magnetoresistance in spin filtering tunnel junctions: Experiment and theory, Phys. Rev. B **76**, 134412 (2007).
[48] B. B. Nelson-Cheeseman, R. V. Chopdekar, L. M. B. Alldredge, J. S. Bettinger, E. Arenholz, and Y. Suzuki, Probing the role of the barrier layer in magnetic tunnel junction transport, Phys. Rev. B **76**, 220410(R) (2007).
[49] M. Gajek, M. Bibes, A. Barthélémy, K. Bouzehouane, S. Fusil, M. Varela, J. Fontcuberta, and A. Fert, Spin filtering through ferromagnetic $BiMnO_3$ tunnel barriers, Phys. Rev. B **72**, 020406(R) (2005).
[50] R. V. Chopdekar, B. B. Nelson-Cheeseman, M. Liberati, E. Arenholz, and Y. Suzuki, Role of magnetic anisotropy in spin-filter junctions, Phys. Rev. B **83**, 224426 (2011).
[51] A. V. Ramos, M.-J. Guittet, J.-B. Moussy, R. Mattana, C. Deranlot, F. Petroff, and C. Gatel, Room temperature spin filtering in epitaxial cobalt-ferrite tunnel barriers, Appl. Phys. Lett. **91**, 122107 (2007).
[52] J. S. Moodera, The phenomena of spin-filter tunneling, J. Phys.: Condens. Matter. **19**, 165202 (2007).
[53] C. Ortiz Pauyac, A. Kalitsov, A. Manchon, and M. Chshiev, Spin-transfer torque in spin filter tunnel junctions, Phys. Rev. B **90**, 235417 (2014).
[54] Y. Yuan and A. Manchon, arXiv:1206.3743 (2012).
[55] M. Wilczyński, Spin-transfer torque in double tunnel junctions with ferromagnetic barriers and nonmagnetic electrodes, J. Magn. Magn. Mater. **325**, 94 (2013).
[56] Y. Cheng, K. Chen, and S. Zhang, Interplay of magnon and electron currents in magnetic heterostructure, Phys. Rev. B **96**, 024449 (2017).
[57] I. Theodonis, N. Kioussis, A. Kalitsov, M. Chshiev, and W. H. Butler, Anomalous Bias Dependence of Spin Torque in Magnetic Tunnel Junctions, Phys. Rev. Lett. **97**, 237205 (2006).
[58] A. Kalitsov, W. Silvestre, M. Chshiev, and J. P. Velev, Spin torque in magnetic tunnel junctions with asymmetric barriers, Phys. Rev. B **88**, 104430 (2013).
[59] M. Wilczyński, J. Barnaś, and R. Świrkowicz, Free-electron model of current-induced spin-transfer torque in magnetic tunnel junctions, Phys. Rev. B **77**, 054434 (2008).
[60] J. C. Slonczewski, Conductance and exchange coupling of two ferromagnets separated by a tunneling barrier, Phys. Rev. B **39**, 6995 (1989).
[61] A. Kalitsov, M. Chshiev, I. Theodonis, N. Kioussis, and W. H. Butler, Spin-transfer torque in magnetic tunnel junctions, Phys. Rev. B **79**, 174416 (2009).
[62] M. Chshiev, A. Manchon, A. Kalitsov, N. Ryzhanova, A. Vedyayev, N. Strelkov, W. H. Butler, and B. Dieny, Analytical description of ballistic spin currents and torques in magnetic tunnel junctions, Phys. Rev. B **92**, 104422 (2015).
[63]

$$\gamma_L^{\uparrow} = \frac{4k_S^2(k_S^2+\kappa^{\downarrow 2})\sqrt{\mathcal{A}}\sin(k_S d_S+\alpha)\sin(k_S d_S+\beta^{\downarrow})}{[\mathcal{A}\sin(2k_S d_S+\xi)+\mathcal{B}\cos\theta-(k_S^2+\kappa^{\downarrow}\kappa^{\uparrow})^2]^2},$$

$$\gamma_L^{\downarrow} = \frac{4k_S^2(k_S^2+\kappa^{\uparrow 2})\sqrt{\mathcal{A}}\sin(k_S d_S+\alpha)\sin(k_S d_S+\beta^{\uparrow})}{[\mathcal{A}\sin(2k_S d_S+\xi)+\mathcal{B}\cos\theta-(k_S^2+\kappa^{\downarrow}\kappa^{\uparrow})^2]^2},$$

$$\gamma_R = -\frac{2k_S^2}{[\mathcal{A}\sin(2k_S d_S+\xi)+\mathcal{B}\cos\theta-(k_S^2+\kappa^{\downarrow}\kappa^{\uparrow})^2]},$$

with $\mathcal{A}=(k_S^2+\kappa^{\downarrow 2})(k_S^2+\kappa^{\uparrow 2})$, $\mathcal{B}=k_S^2(\kappa^{\downarrow}-\kappa^{\uparrow})^2$, $\alpha=\tan^{-1}\left[(k_S(\kappa^{\downarrow}+\kappa^{\uparrow}))/(\kappa^{\downarrow}\kappa^{\uparrow}-k_S^2)\right]$, $\beta^{\sigma}=\tan^{-1}\left[2k_S\kappa^{\sigma}/(\kappa^{\sigma 2}-k_S^2)\right]$, and $\xi=\tan^{-1}\left[((k_S^2-\kappa^{\downarrow}\kappa^{\uparrow})^2-k_S^2(\kappa^{\downarrow}+\kappa^{\uparrow})^2)/(2k_S(\kappa^{\downarrow}+\kappa^{\uparrow})(k_S^2-\kappa^{\uparrow}\kappa^{\downarrow}))\right]$.
[64] P. V. Lukashev, A. L. Wysocki, J. P. Velev, M. van Schilfgaarde, S. S. Jaswal, K. D. Belashchenko, and E. Y. Tsymbal, Spin filtering with EuO: Insight from the complex band structure, Phys. Rev. B **85**, 224414 (2012).
[65] J. Marschall and A. Majumdar, Charge and energy transpot by tunneling thermoelectric effect, J. Appl. Phys. **74**, 4000 (1993).

[66] M. Wilczyński, Thermopower in double planar tunnel junctions with ferromagnetic barriers and nonmagnetic electrodes, J. Magn. Magn. Matter. **421**, 418 (2017).

[67] H. Jang, L. Marnitz, T. Huebner, J. Kimling, T. Kuschel, and D. G. Cahill, Thermal Conductivity of Oxide Tunnel Barriers in Magnetic Tunnel Junctions Measured by Ultrafast Thermoreflectance and Magneto-Optic Kerr Effect Thermometry, Phys. Rev. Appl. **13**, 024007 (2020).

[68] A. Kalitsov, A. Coho, N. Kioussis, A. Vedyayev, M. Chshiev, and A. Granovsky, Impurity-Induced Tunning of Quantum-Well States in Spin-Dependent Resonant Tunneling, Phys. Rev. Lett. **93**, 046603 (2004).

[69] B. S. Tao, H. X. Yang, Y. L. Zuo, X. Devaux, G. Lengaigne, M. Hehn, D. Lacour, S. Andrieu, M. Chshiev, T. Hauet, F. Montaigne, S. Mangin, X. F. Han, and Y. Lu, Long-Range Phase Coherence in Double-Barrier Magnetic Tunnel Junctions with a Large Thick Metallic Quantum Well, Phys. Rev. Lett. **115**, 157204 (2015).

[70] B. Tao, C. Wan, P. Tang, J. Feng, H. Wei, X. Wang, S. Andrieu, H. X. Yang, M. Chshiev, X. Devaux, T. Hauet, F. Montaigne, S. Mangin, M. Hehn, D. Lacour, X. Han, and Y. Lu, Coherent resonant tunneling through double metallic quantum well states, Nano Lett. **19**, 3019 (2019).